Journal of Loss Prevention in the Process Industries 71 (2021) 104510

Contents lists available at ScienceDirect

Journal of Loss Prevention in the Process Industries

journal homepage: http://www.elsevier.com/locate/jlp

Characterization of a medium velocity deluge nozzle for offshore installations

Joachim Lundberg

University of South-Eastern Norway, Kjolnes Ring 56, 3918, Porsgrunn, Norway

ARTICLE INFO

Keywords:
NORSOK
Deluge spray
Shadow imaging
Linear patternator

ABSTRACT

It is important to study the characteristics of the nozzle of the deluge spray to comply with the standards developed by the petroleum industry for offshore installations in Norway. Due to the stochastic nature of the decomposition processes and geometrical features within the nozzle, the deluge spray has a complex flow field. Since the flow field determines the performance of the spray, the present study performs an experimental characterization of a medium velocity deluge nozzle for validation of computational fluid dynamics (CFD) models. The experiment was conducted for a maximum supply water pressure of 8.0 bar (g), which is identical to the operating pressures of offshore installations. Formerly, characterization studies of deluge or sprinkler spray were mostly targeted on residential usage with lower supply water pressures. I utilized a laser-based shadow imaging system to capture high-speed images, which were later processed in MATLAB. A linear patternator was used to validate the results of the shadow imaging technique. The geometrical features of the deluge nozzle played an important role in determining the characteristics of the spray. In addition, the supply water pressure significantly affected the size and velocity distributions of the droplets, applied density (volume flux), and area coverage. However, the Sauter mean diameter did not vary significantly with the azimuthal or radial position of the droplet within the inner region of the spray. The measurements obtained in this study can be used to estimate the extinguishing efficiency of a deluge system for offshore installations with elevated supply water pressures. Deviations between measurements with shadow imaging and patternator technique are discussed and discrepancies are discussed.

1. Introduction

The Norwegian petroleum industry has developed standards to ensure adequate safety, value addition, and cost-effectiveness following the accidents on the Norwegian continental shelf. The NORSOK S-001 (NORSOK S-001, 2018) standard has been instituted for the technical safety of offshore installations. This guideline specifies that a source of quick and reliable firewater supply should be available for applicable deluge/firewater spray systems at a rate that is sufficient to meet the minimum demands for the applicable area and at a pressure that satisfies the nozzle pressure range requirements. The deluge system shall provide adequate coverage for the relevant fire and explosion scenarios in terms of both volume and area as well as equipment coverage. The standard also specifies that the minimal water densities (volume flux) shall be equal to $10(dm^3/\text{min})/m^2$ for process areas and equipment surfaces and $20(dm^3/\text{min})/m^2$ for wellheads. The deluge system is designed according to the NFPA 15 standard (Bell, 2017). Chapter 6.2.4 of the NEPA 15 standard describes the criteria that must be followed while positioning the deluge nozzles. This standard discusses the extinguishing properties of the deluge system. The guidelines discuss the nozzle design, characteristics of the produced water spray pattern, effect of the nozzle orientation on the coverage characteristics, and impact of the wind and fire draft on very small droplets and large droplets with minimal initial velocities.

The droplet size plays an important role in the design of the deluge system. A determinant quantity refers to the size distribution of the droplets. The small droplets can quench combustion and cool fire gases without penetrating the fire plume. However, the weather conditions at the offshore installation's open structure direct the small droplets away from the desired regions. In contrast, large droplets have a higher momentum, which allows them to reach the origin of the fire and successfully cool the process equipment (Wighus, 2012).

Despite several studies on the size distribution and break-up mechanisms of the deluge spray, little information is available on the detailed properties of a specific nozzle. Jackman (1992) manually measured the droplet sizes and velocities for some commercial nozzles through

E-mail address: Joachim.Lundberg@usn.no.

https://doi.org/10.1016/j.jlp.2021.104510
Received 22 January 2021; Received in revised form 12 March 2021; Accepted 13 April 2021
Available online 17 April 2021

photographic high-speed film images. The study characterized residential nozzles for fire sprinklers, but the obtained results were manually measured and dependent on the operator of the system. Sheppard (2002) categorized the droplet sizes and velocity fields by using phase Doppler anemometry (PDA) and particle image velocimetry (PIV), respectively. The study aimed to find characteristics of residential fire water nozzles for computational use.

Zhou et al. (2012) used a laser-based shadow imaging technique to characterize sprinkler spray systems. The near-field measurements carried out in the study were based on numerical fire models. An array of water collectors, equipped with pressure transducers, aided the validation of the volume-flux values used in the shadow imaging technique.

Zlatanovic et al. (2014) characterized residential sprinkler spray systems at low water pressures. They observed that the droplet distribution was heavily dependent on the sprinkler geometry. In addition, the initial spray characteristics displayed a weak dependence on the water temperature. The calculated and experimentally determined droplet sizes were found to be identical after making some assumptions.

Myers and Marshall (2016) and Beji et al. (2018) utilized the results from (Ren et al., 2011; Zhou, 2015; Zhou et al., 2012) to develop a Euler–Lagrangian representation of the sprinkler spray in a CFD environment. Beji et al. (2018) developed an accurate sprinkler spray model for hot air jets using a CFD software named Fire Dynamic Simulator (FDS). The study conducted by Myers and Marshall (2016) provided an initial description for the spray model that was based on statistical theory. They utilized the data from the same experimental setup as that used by Jordan et al. (2017) and Link et al. (2017). This study provided an implementation framework for spray models and application guidance for the CFD software FireFOAM.

Conventionally, offshore installations operate at higher supply water pressures than residential sprinkler systems (Roberts, 2004). Thus, the characteristics of the deluge spray for offshore and residential systems may be dissimilar.

A medium velocity deluge nozzle, commonly used in offshore installations, was characterized for pressures up to 8.0 bar (g) in this study. A laser-based shadow imaging technique with image processing was used to categorize the deluge nozzle after validating the results with the data obtained from the patternator experiments. The results were simplified and expressed as CFD input values. Attempts were made to ensure that the applications of this study complied with the NORSOK S-001:2018 standard (NORSOK S-001, 2018).

2. Materials and methods

A medium velocity deluge nozzle (Tyco MV34-110) with a K-factor of 58.8 L/(min $\times$ $\sqrt{\text{bar}}$) was used in the current study to represent a deluge spray for offshore applications. The measurements were taken outside the primary break-up region in a horizontal plane, 1.00 m below the nozzle. The location was chosen as a reference location for later CFD implementation.

A laser-based shadow imaging technique was used to obtain the spray characteristics. The raw images were processed in MATLAB 2019b. This technique captured highly magnified images and extracted the data from every individual frame at different positions of the spray. A linear patternator was used to compare the experimentally obtained results with the actual volume flow and volume flux of the water in the spray.

The experiments were performed in a container with a length, width, and height of 5.2 m, 2.4 m, and 2.4 m, respectively, in the process safety and gas explosion laboratories at the University of South-Eastern Norway in Porsgrunn. The experiments were conducted from 2014 to 2020.

2.1. Experimental setup

The experimental setup used to measure the spray characteristics is shown in Fig. 1. A continuously pulsed copper vapor laser (Oxford lasers LS 20–50) was used to produce ~2 mJ/pulse of light at constant wavelengths of 511 nm and 578 nm. The laser beam was transferred through a 20 m optical fiber cable to a 100 mm collimating beam expander lens equipped with a diffusor plate. A high-speed camera (Photron APX-RS), equipped with a long-distance microscope lens (Questar QM-1), captured the expanded laser beam in a backlit formation. The camera was focused at a point 1.00 m below the nozzle. The distance between the camera lens and the focal point was approximately 1.0 m. The distance between the camera lens and the light diffusor for the laser light was approximately 2.0 m. The resolution of the camera was 512 $\times$ 416 pixels (at 12500 frames per second) and provided a field of view (FOV) for the setup that measured 10.8 mm $\times$ 8.7 mm. The spray did not contain any screening or splash guards to preserve the flow field of the spray. The camera and laser were synchronized to capture images at intervals of 80 μs.

Spatial calibration was performed with a reticle (Patterson globe and a 1.5 mm sphere). The depth of field (DOF) was obtained by traversing the reticle in a plane perpendicular to the field of view of the camera. The relationship between the DOF of the i^{th} droplet DOF_i and droplet

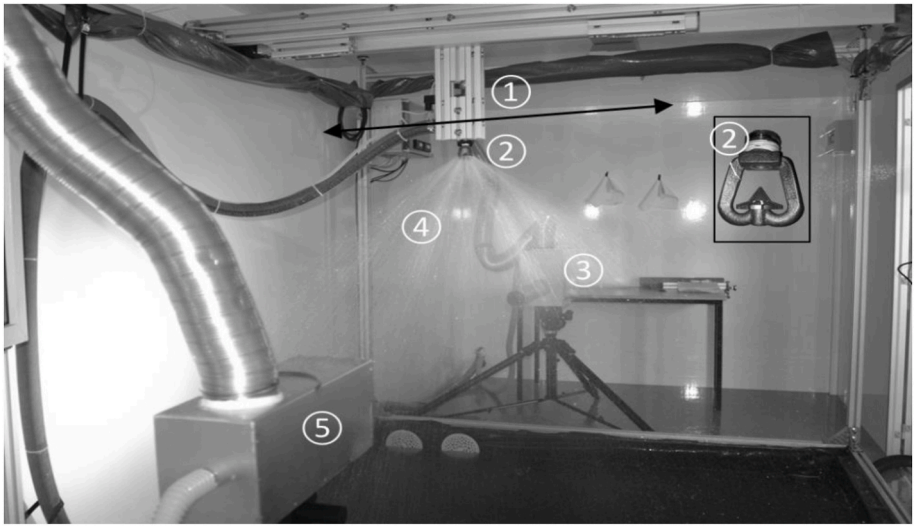

Fig. 1. Experimental setup: 1) traverse with nozzle mounting, 2) deluge nozzle, 3) high-speed camera with a long-distance microscope lens, 4) deluge spray, and 5) laser transmitting optics.

diameter d_i is given as $DOF_i = 24 \cdot d_i$. The sizes and velocities of approximately 2000 droplets were measured at every point in the spray to ensure the reliability of the results. The following section explains the image processing algorithm used in the measurements.

According to the calibration of the sizing standard used in this study, the percentage of uncertainty in the measurement method was capped at approximately 10%. Lundberg (2015) has explained the measurement procedure in greater detail.

The specifications of the medium velocity deluge nozzle are listed in Table 1.

The linear patternator used to verify the data, as shown in Fig. 2), consisted of fifteen 10 mm acrylic cylinders placed side-by-side. The internal diameter and height of each cylinder were 9.4 mm and 450 mm, respectively. The patternator was designed to collect water droplets at the same locations as those of the shadow imaging technique (except at 150 cm). A digital weight and timer measured the actual volume flux of the supplied water.

The spatial location of the measurements was in a circular horizontal plane 1.0 m below the tip of the nozzle. The plane was represented in polar coordinates by the radius from the center of the spray (r) and the azimuthal angle (φ), where the frame arm was equal to 0°.

Fig. 3 shows the locations of the measurement points that have been listed in Table 2.

2.2. Image processing

The image-processing algorithm was developed by using the image processing toolbox in MATLAB (Mathworks, 2019). A combination of established and novel image processing techniques was used to extract information about the deluge spray from the shadow images. The droplet sizes and droplet velocity varied from 100 μm to 3000 μm and 0 m/s to 30 m/s, respectively.

The shadow images consist of droplets (both "in-focus" and "out-of-focus"), noise, and the background. The background refers to an image without any droplets or noise. In an ideal shadow image, the "in-focus" droplets are black, the "out-of-focus" droplets are gray, and the background is white, thereby making it is easy to identify the "in-focus" droplets. However, due to varying illumination and optical aberrations in actual experiments, the background appears to be uneven, and there are only minor differences between "in-focus" to "out-of-focus" droplets. An original image obtained from one of the shadow imaging experiments is shown in Fig. 4a.

Due to spatially uneven illumination and interference patterns, the backgrounds of the images need to be corrected. An estimate of the variable background can be obtained by averaging all the measurement frames according to Eq. (1).

$$B = \frac{1}{n}\sum_{i=1}^{n} I_i. \tag{1}$$

The above equation is obtained by assuming a low droplet density (<10% area based). The difference between the background and an original image yields a corrected image, independent of uneven illumination and interference patterns. The corrected image and background estimate are shown in Fig. 4a and 4c, respectively.

A threshold algorithm binarizes the image into droplets and background (including noise). The popular Otsu algorithm (Otsu, 1979) was used to calculate the threshold value t. The algorithm maximizes the inter-class variance between the droplets and the background (Gonzalez et al., 2009). The threshold value converts the grayscale image ji (x, y) into background and droplets, where (x, y) represents the pixel coordinates. The output of the threshold algorithm is a binary image, i.e., droplets and background, as shown in Fig. 4d.

Although the threshold algorithm isolates the droplets, false readings (out-of-focus droplets, background noise, droplets in front of each other, and droplets with uneven edges) may still exist. A distinction between real droplets and false readings can be performed by accounting for the droplet shape. An object recognition algorithm is applied to the droplets to measure the properties. A visual consideration of the droplets suggests that the characteristic feature of a non-real droplet (false reading) is either an uneven edge or a non-circular shape. The non-real droplets are excluded before studying the characteristics of the spray, as shown in Fig. 4e. The droplet qualification algorithm is described in (Lundberg, 2015).

The droplet diameter is calculated by Eq. (2) on the area containing the isolated droplets.

$$d_i = \sqrt{4A/\pi}. \tag{2}$$

The velocity is measured by comparing each droplet's position in a given frame with the position of the same droplet in subsequent frames, as shown in Fig. 4f. The technique is based on an assignment problem described by Lundberg and Lysaker (2015).

Table 1
Specifications for the medium velocity deluge nozzle.

Parameter	Units	Value
Orifice diameter	mm	9.6
Discharge coefficient	$dm^3/(min \times \sqrt{bar})$	58.8
Dispersion angle	°	110.0
Working pressure range	bar (g)	1.4–12.1

Fig. 2. Measurement of the actual water flow/flux by using a patternator.

3. Theory

The deluge spray is often represented in CFD software by Lagrangian particles introduced to a continuous Eulerian phase. A Lagrangian-Eulerian approach is adopted for such problems. The continuous phase (combustion gas or air) is modeled as a Eulerian field by a control volume method. The droplets are modeled by using Lagrangian droplet tracking. The initial droplet size and velocity field of the Lagrangian particles are determined either by a model or experimentally. Due to the stochastic nature of the decomposition of the droplets and the deluge nozzle's geometrical features, a non-homogeneous flow field is expected and averaged for all parameters (size and velocity distribution and applied volume flux).

The results of the shadow imaging technique are obtained by combining droplet data at different locations in the spray. One of the disadvantages of using the shadow imaging technique was that a large

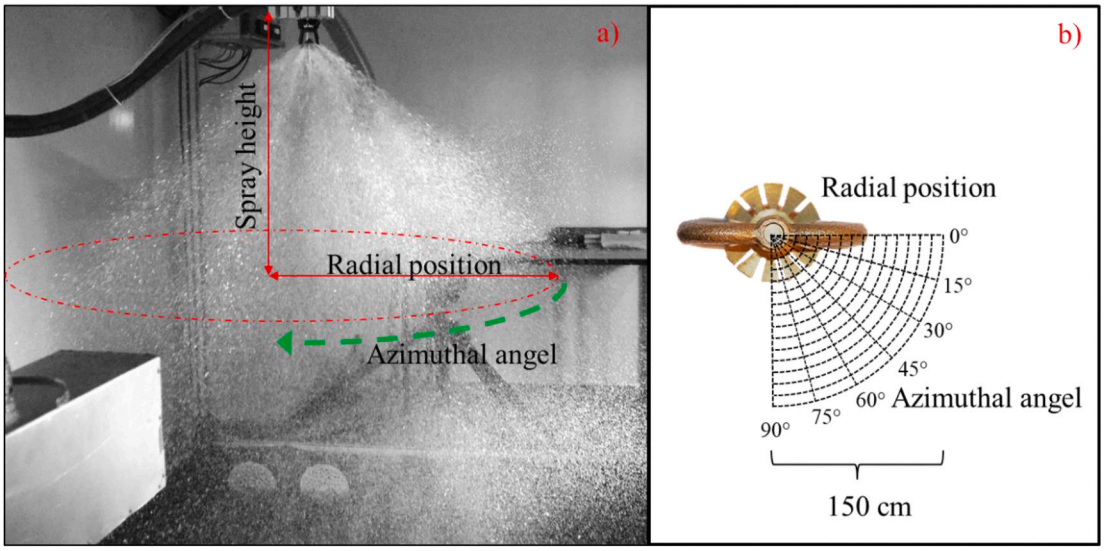

Fig. 3. a) Schematic of the measurement directions in the setup. b) Locations of the measurement points.

Table 2
Range of the experiments.

	Range	Interval
Supply water pressure	2.0–8.0 bar (g)	3.0 bar
Radial distance	0–150 cm	10 cm
Azimuthal angle	0–90°	15°

droplet had a larger depth of field and smaller field of view than those of a small droplet. This effect was compensated for by using a statistical weight.

The statistical weight (SW_i) for the i^{th} droplet is represented by the following equations.

$$SW(Border_i) = FOV_i = \frac{W \cdot H}{(W - d_i) \cdot (H - d_i)}, \tag{3}$$

$$SW(DOF_i) = \frac{d_{ref}}{\mathrm{DOF}_i}, \tag{4}$$

$$SW_i = SW(DOF_i) \cdot SW(\mathrm{Border}_i). \tag{5}$$

d_{ref} is the reference droplet diameter, and DOF_i represents the depth of field for the i^{th} droplet. W and H represent the width and height of the field of view, respectively (extent of the images) (Kashdan et al., 2003).

The Sauter mean diameter (d_{32}) is an indicator of the flow properties for the deluge spray. It is known to be descriptive for mass transfer and chemical reactions (Lefebvre and Mcdonell, 2017). The Sauter mean diameter is equal to the ratio of the sum of the volume of the droplets to the sum of their surface areas. This quantity has a volume to surface area ratio that is identical to that of the whole spray (Grant et al., 2000). d_{32} is calculated using Eq. (6).

$$d_{32} = \frac{\sum SW_i \cdot (d_i)^3}{\sum SW_i \cdot (d_i)^2}. \tag{6}$$

The mass-averaged velocity v_{MA} represents the velocity distribution of the droplets and is calculated by using Eq. (7).

$$v_{MA} = \frac{\sum SW_i \cdot (d_i)^3 \cdot v_i}{\sum SW_i \cdot (d_i)^3}, \tag{7}$$

where v_i is the velocity of the i^{th} droplet.

The averaged applied water flux is equal to the amount of water per area per unit time and can be calculated by feeding the data from the images into Eq. (8).

$$\dot{q}_{flux} = \left(\sum_{1}^{N} \frac{\pi d_i^3 \cdot v_i \cdot \cos(\phi)}{6 FOV_i \cdot DOF_i} \right) \frac{1}{N}, \tag{8}$$

where ϕ represents the direction of the droplets in the vertical axes, and N is the total number of frames. The procedure is similar to that adopted by Zhou et al. (2012). However, the expression in the current study are modified to consider the measurements in a plane 1.0 m below the nozzle. Further, Zhou et al. (2012) performed measurements spherically from the nozzle. The current study performs measurements linearly in a plane below the nozzle.

The frequency of the measured droplet diameters is divided into three droplet size (diameter) intervals, namely small, medium, and large droplets, which is similar to the procedure adopted by Myers et al. (2018). However, the range values are modified because the current spray is meant for offshore applications that operate at higher pressures. The intervals are listed in Table 3.

The volume flow of water is calculated by interpolating the applied volume-flux measurements to a polar coordinate system and multiplying them with their respective area value. The azimuthal contributions are then summarized to obtain the radial volume-flow distribution of water in volume per unit length.

$$Q_{j=0\to150} = 4 \cdot \sum_{\varphi=0^\circ}^{\varphi=90^\circ} \dot{q}_{\varphi,j} \cdot A_{\varphi,j}. \tag{9}$$

The total volume flow of water is equal to the sum of the radially distributed flows.

$$Q = \sum Q_{j=0\to150}. \tag{10}$$

4. Results and discussion

A complete characterization of a medium velocity deluge nozzle (Tyco MV34-110) was performed for a water supply pressure of 2.0, 5.0, and 8.0 bar (g). The purpose of this study was to calculate the averaged spray parameters to validate CFD models.

Due to the nozzle's geometrical features and the stochastic nature of the break-up processes occurring within the deluge nozzle, the size and velocity distributions varied across the control volume of the spray. The size-dependent droplet velocity was proved to be dependent on the location as well. Fig. 5a shows the droplet size distribution at one point of the spray. Fig. 5b shows the size-dependent velocities of the droplets

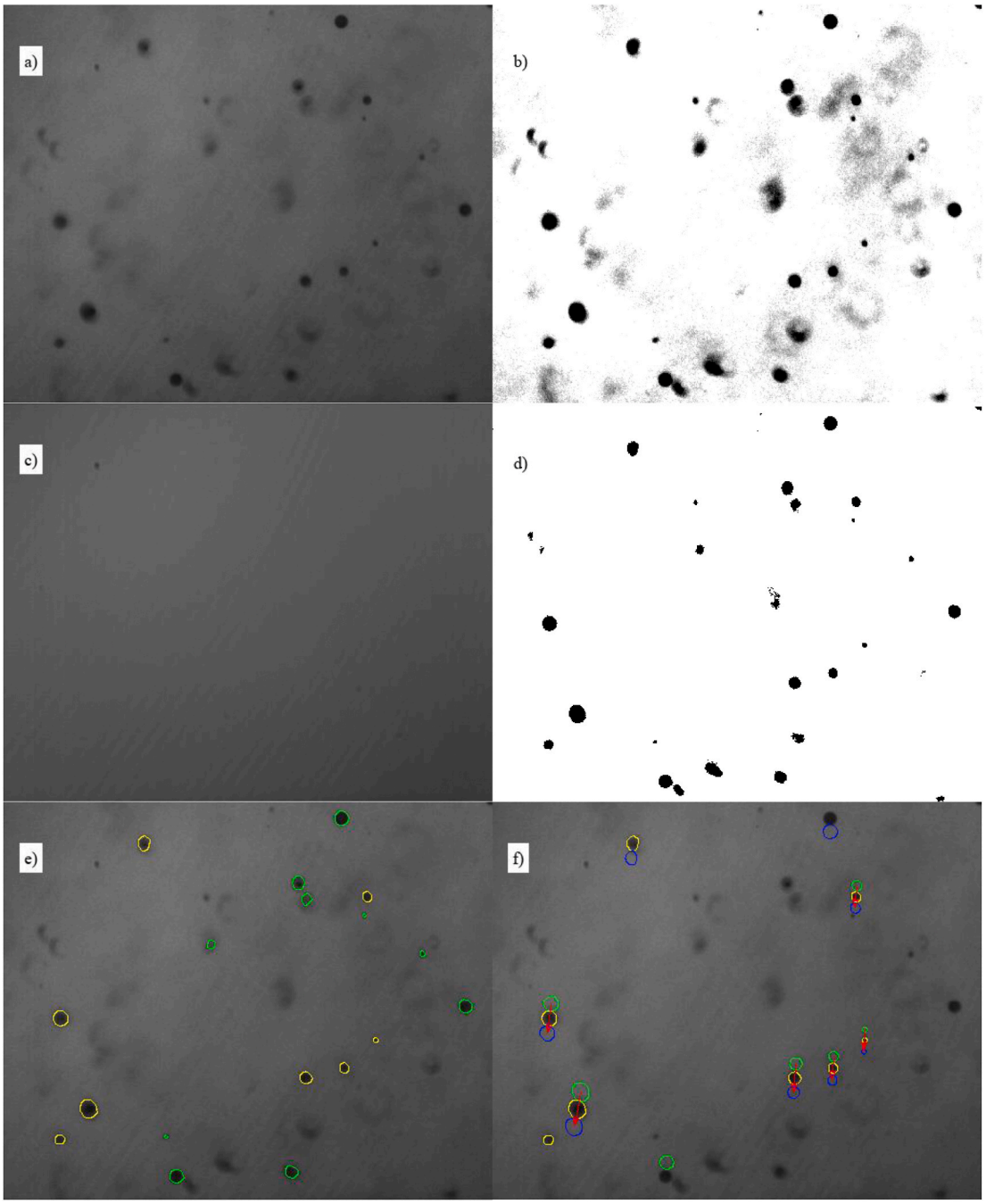

Fig. 4. a) Original image I_i, b) background-subtracted image J_i obtained by using Eq. (1), c) background B, d) thresholded image T_i, e) qualified droplets, and f) velocity field.

Table 3
Droplet size categories for deluge water droplets.

Small	$d_i<300$
Medium	$300<d_i<600$
Large	$600<d_i$

at the same point.

The results indicate that the size distribution at this point had a Rosin–Rambler shape. The size-dependent droplet velocity increases with increasing droplet diameter.

As a result, it was impractical to document the droplet size and velocity distributions at all locations in the spray. The normalized frequencies of the small, medium, and large droplets are given for different radial positions in the spray and averaged for the azimuthal angle. Fig. 6a, 6b, and 6c present the variation in the normalized frequencies of the droplet sizes with the radial position for different supply water pressures.

The figures show that the normalized frequencies of the small droplets were lower at 2.0 bar (g) than they were at 5.0 bar (g) and 8.0 bar (g). In addition, the number of large droplets decreased with increasing pressure.

Variation in the Sauter mean diameter with the radial position for different azimuthal angle and supply water pressures is shown in Fig. 7a, 7b, and 7c.

The Sauter mean diameter was found to decrease with reducing supply water pressures. However, the Sauter mean diameter increased

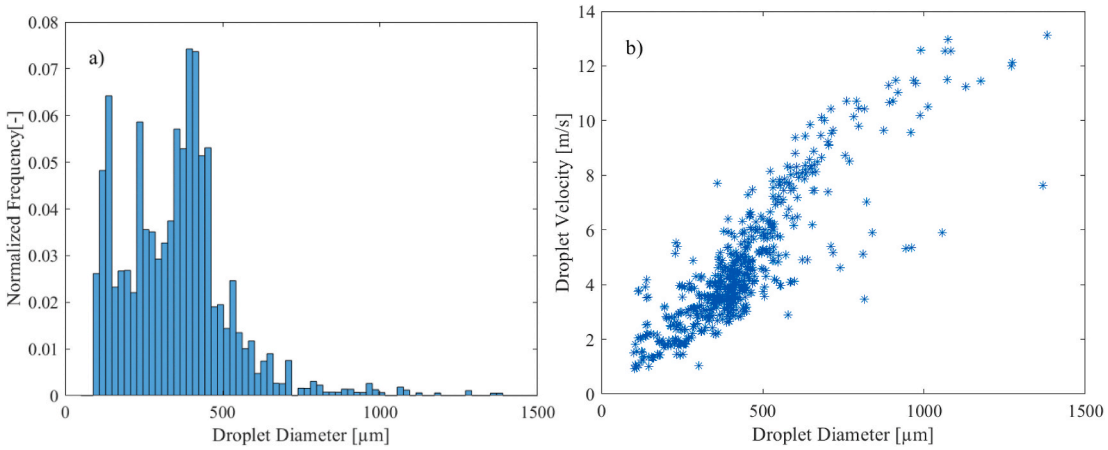

Fig. 5. (a) The diameter (b) and velocity of the local droplet distribution for a supply water pressure of 2.0 bar (g) at a radial location of 80 cm and an azimuthal angle of 45°.

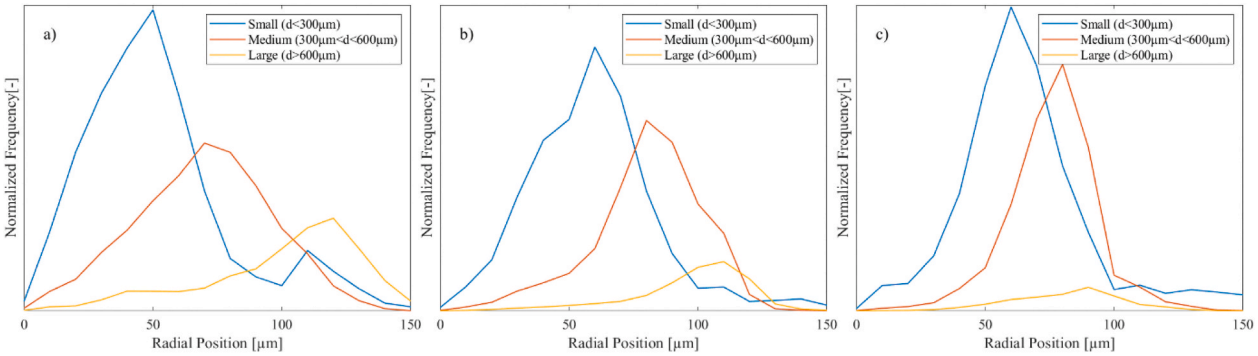

Fig. 6. Variation in the normalized frequencies of the droplet sizes with the radial position for supply water pressures of a) 2.0 bar (g), b) 5.0 bar (g), and c) 8.0 bar (g).

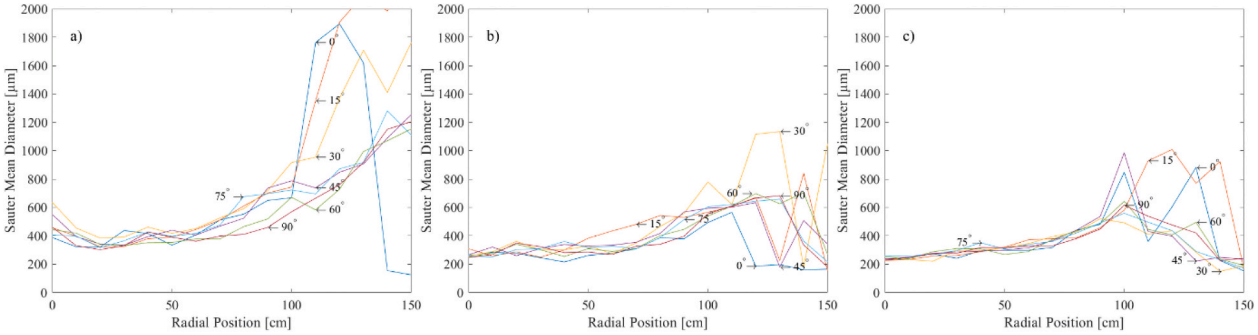

Fig. 7. Variation in the Sauter mean diameter of the droplets with their radial position for different azimuthal angles at supply water pressures of a) 2.0 bar (g), b) 5.0 bar (g), and c) 8.0 bar (g).

with increasing radial distance. The smaller droplets were dominant in the center of the spray, while the large droplets dominated the outer regions. The Sauter mean diameter was significantly affected by large, individual droplets that impacted the stability of the results in regions with few droplets ($r > 100\ cm$).

Fig. 8 shows the dependence of the mass-averaged velocity on the droplet size. The velocity was averaged to compensate for deviations in the velocity due to different droplet sizes. Variation in the mas-averaged velocity with the radial position for different water supply pressures is shown in Fig. 8a, 8b, and 8c.

The mass averaged velocity varies with the azimuthal angle and radial position of the droplets. Most droplet velocities ranged from 4 m/s to 10 m/s and increased gradually with increasing supply water pressure. However, some geometrical dependencies can be observed on the measurements following the nozzle tines (15°, 45°, and 75°) compared to the measures following the slots (0°, 30°, 60°, and 90°). This variation was absent at the highest supply water pressure.

Fig. 9a and 9b shows the variation in the volume flow and volume flux with the radial position at different supply water pressures. The spray was found to have a higher coverage at lower supply water pressures.

The volume-flow distribution of the water, measured with the shadow imaging technique, is compared with the flow distribution measurements of the linear patternator in Fig. 10a, 10b, 10c.

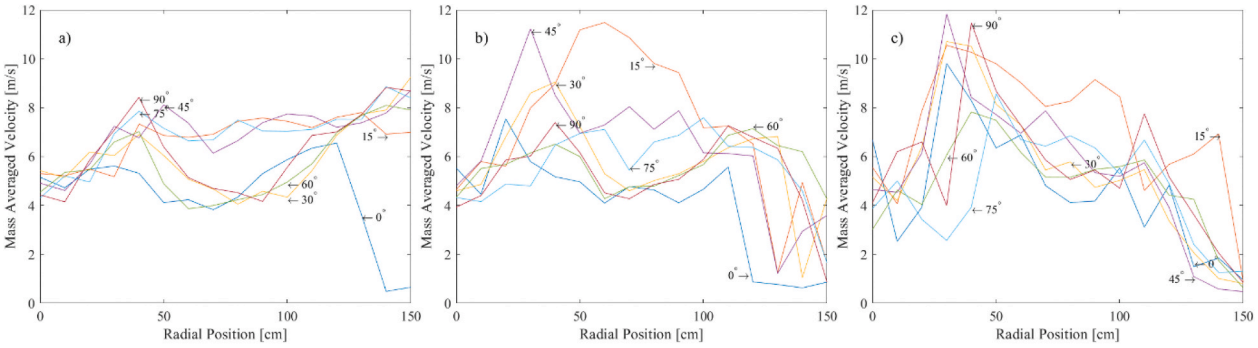

Fig. 8. Variation in the mass-averaged velocity of the droplets with the radial position for different azimuthal angles at supply water pressures of a) 2.0 bar (g), b) 5.0 bar (g), and c) 8.0 bar (g).

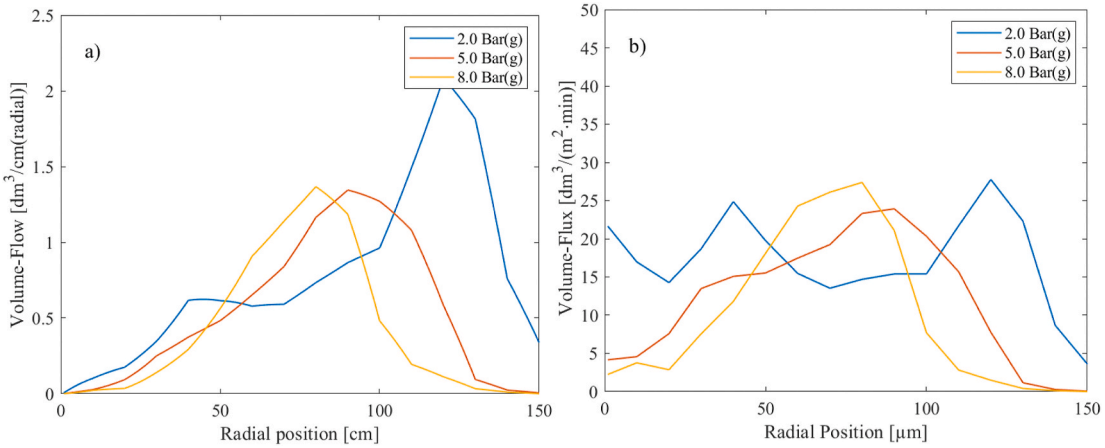

Fig. 9. Variation in a) volume flow and (b) applied volume flux of the water with the radial position.

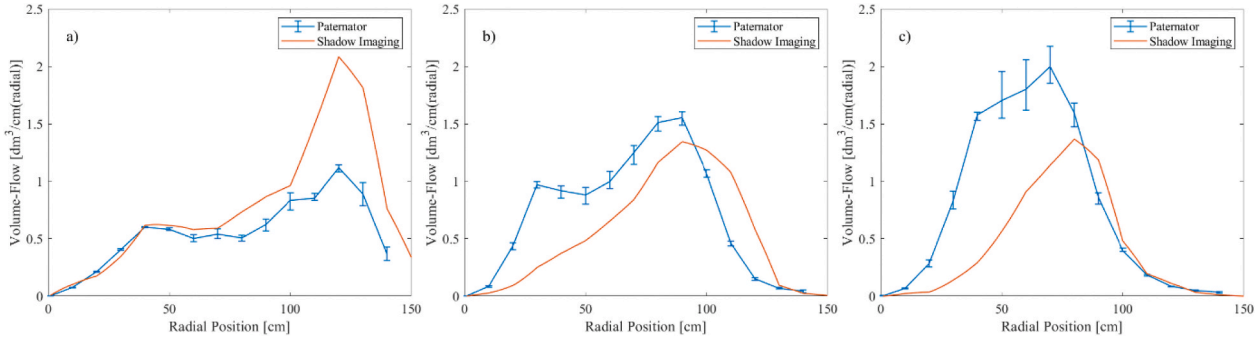

Fig. 10. Comparison of the variation in the volume flow of the water with the radial position obtained by the shadow imaging technique and the patternator for supply water pressures of a) 2.0 bar (g), b) 5.0 bar (g), and c) 8.0 bar (g).

Fig. 10 shows that the shadow imaging technique underpredicted the volume flow at high supply water pressures within the inner regions of the spray due to low visibility. In addition, the shadow imaging technique also overpredicted the volume flow in the outer areas of the spray, which is attributed to the interference between droplets from different azimuthal angles. Both techniques show the water flow to be distributed more closely to the inner regions for the higher supply water pressures. The 5.0 bar (g) measurements give the most homogeneous flow distribution of the three series. The area coverage of the spray is increasing with decreasing supply water pressure, while the volume flow increases with increasing pressure.

The results of the measurement of the applied volume flux with the shadow imaging technique for the different supply water pressures are shown in Fig. 11a, 11b, and 11c.

The applied volume flux was dependent on the radial and azimuthal positions of the droplet in the spray. The increasing supply water pressure was found to have a negative impact on the area coverage, thereby narrowing the spray. The geometrical features of the nozzle influenced the spray pattern by producing a non-homogeneous applied volume flux.

The actual volume flux was measured by a linear patternator to validate the results of the shadow imaging technique. The results are shown in Fig. 12a, 12b, and 12c.

The actual delivered volume flux of the water, measured by the linear patternator, demonstrated similar tendencies to that measured by the shadow imaging technique. However, the former technique

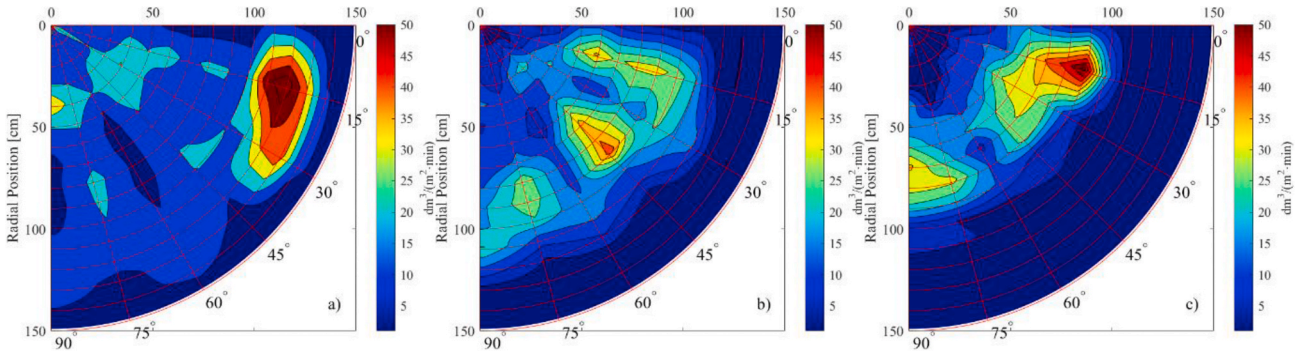

Fig. 11. Measurement of the applied volume flux of the water with the shadow imaging technique for supply water pressures of a) 2.0 bar (g), b) 5.0 bar (g), and c) 8.0 bar (g).

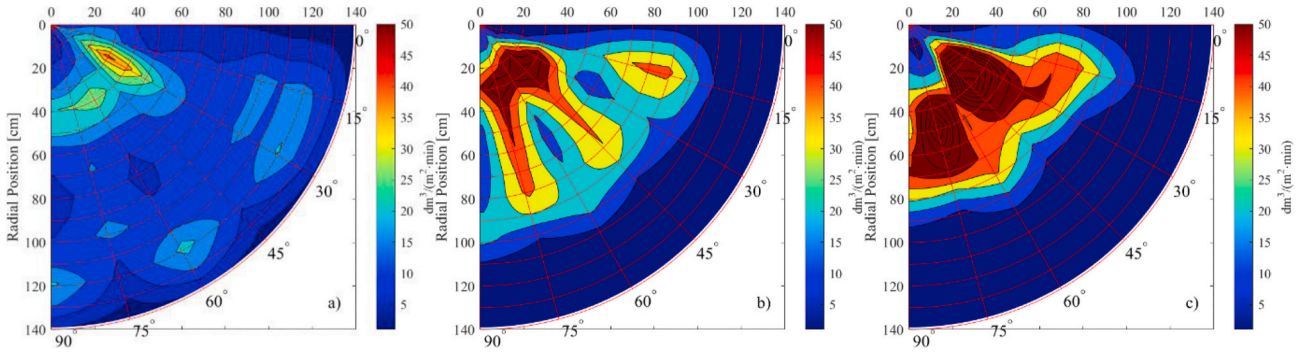

Fig. 12. Measurement of the actual volume flux of the water with the patternator for supply water pressures of a) 2.0 bar (g), b) 5.0 bar (g), and c) 8.0 bar (g).

indicated the presence of high flux zones in the inner regions of the spray, which were absent in the measurements obtained by the latter.

Comparing results obtained by the patternator represents the total volume of the water delivered to a specific location in the flow, and is sufficient to fulfill the demand of a minimum applied water flux. However, in the case of a scenario with fire or windy conditions the velocity and droplet size is important parameters and are impossible to obtain with such a technique.

Table 4 compares the total amount of water calculated using the shadow imaging technique and the linear patternator with the amount of water entering the nozzle.

The total amount of water listed in Table 4 shows the shadow imaging method to deviate from the amount of water entering the nozzle due to the droplet density in the inner region of the spray in the 5.0 bar (g) and 8.0 bar (g) run. For the 2.0 bar (g) run, the amount deviates due to the overprediction of the large droplets in the outer regions of the spray. Nevertheless, the Sauter mean diameter for the three supply water pressures shown in Fig. 7a, 7b, and 7c have consistent values for the mean diameters in the inner regions of the spray. This implies that the droplet size distribution is not skewed by the measurement method. The measurements with the patternator deviate less from the amount of water entering the nozzle and can be adjusted to give the same total flow by assuming the distribution of water is the same.

Table 4
Comparison of the total amount of water calculated by the shadow imaging technique and linear patternator with the amount of water entering the nozzle.

Pressure	Supply water flow [kg/min]	Patternator [kg/min]	Shadow imaging [kg/min]
2.0 bar(g)	80	79	119
5.0 bar(g)	126	104	83
8.0 bar(g)	161	115	65

5. Conclusion

A laser-based shadow imaging system and a linear patternator were used to characterize the spray emitted from a medium velocity deluge nozzle. The supply water pressures were identical to the pressure values expected in offshore oil and gas installations. The results obtained from the shadow imaging system were compared with the data obtained from the linear patternator. A reasonable agreement was found between the results obtained from the two methods for most of the spray considering Fig. 10.

The geometrical features of the nozzle were found to affect the water distribution of the spray. However, the Sauter mean diameter did not vary significantly with the azimuthal and radial positions of the droplets in the inner region of the spray. The small droplets were dominant in the inner regions of the spray, while the larger droplets dominated the outer regions of the spray.

Considering the extinguishing properties of the spray, present study demonstrated that the droplet size reduced and the droplet velocity increased with increasing supply water pressure. In addition, the area coverage was reduced with increasing pressure. However, the total amount of water increased with increasing supply water pressure. Interestingly, the area coverage was less even at low supply water pressures and indicated dependencies on the geometrical features of the nozzle.

The measurements were taken 1.00 m below the nozzle in the current study and need to be extrapolated at different locations in applications where the nozzles are placed at greater distances from the process equipment and vessels. The area coverage is estimated to increase with decreasing supply water pressure in these cases.

The data obtained from this study can be utilized for practical risk assessments in the actual environment. These data can be utilized by CFD software to simulate the weather conditions and physical properties of the process equipment. Complex spray measurements are not feasible

to recreate in a CFD analysis, but the experimental work in this study can give the CFD programmer information of the extends of the simplifications that are made. Reported measurements point out area coverage, droplet size, and velocity measurement of deluge spray that can be adopted to safety policy for offshore rigs in addition to current minimal volume flux demand.

The major limitation of the shadow imaging method is droplet density. Future development of the measurement technique can be to measure in far-field regions following the spray. This reduces the spray density and reduces the number of droplets removed by the shadow imaging technique due to improper readings.

Author contribution

All research was performed by single author.

Funding

This work was supported by Equinor ASA, Stavanger, Norway [Call-off no 4502094155].

Declaration of competing interest

The authors declare that they have no known competing financial interests or personal relationships that could have appeared to influence the work reported in this paper.

Acknowledgments

I would like to thank Dag Bjerketvedt, Knut Vågsæther, and Marius Lysaker for their unwavering support and guidance throughout this study.

References

Beji, T., Ebrahimzadeh, S., Maragkos, G., Merci, B., 2018. Numerical modelling of the interaction between water sprays and hot air jets - Part II: two-phase flow simulations. Fire Saf. J. 96, 143–152. https://doi.org/10.1016/j.firesaf.2018.01.006.

Bell, K.M., 2017. NFPA 15: Standards for Water Spray Fixed Systems for Fire Protection.

Gonzalez, R.C., Woods, R.E., Masters, B.R., 2009. Digital image processing, third edition. J. Biomed. Opt. https://doi.org/10.1117/1.3115362.

Grant, G., Brenton, J., Drysdale, D., 2000. Fire suppression by water sprays. Prog. Energy Combust. Sci. 26, 79–130. https://doi.org/10.1016/S0360-1285(99)00012-X.

Jackman, L.A., 1992. Sprinkler Spray Interactions with Fire Gases. South Bank University.

Jordan, S.J., Ryder, N.L., Repcik, J., Marshall, A.W., 2017. Spatially-resolved spray measurements and their implications. Fire Saf. J. 91, 723–729. https://doi.org/10.1016/j.firesaf.2017.03.007.

Kashdan, J.T., Shrimpton, J.S., Whybrew, A., 2003. Two-phase flow characterization by automated digital image analysis. Part 1: fundamental principles and calibration of the technique. Part. Part. Syst. Char. 20, 387–397. https://doi.org/10.1002/ppsc.200300897.

Lefebvre, A.H., Mcdonell, V.G., 2017. Atomization and Sprays, second ed. CRC Press, Taylor and Francis. https://doi.org/10.1016/0009-2509(90)87140-N.

Link, E., Myers, T., Trouvé, A., Marshall, A., 2017. Measurements of spray-plume interactions for model validation. Fire Saf. J. 91, 714–722. https://doi.org/10.1016/j.firesaf.2017.04.024.

Lundberg, J., 2015. Image-Based Sizing Techniques for Fire Water Droplets. Telemark University College.

Lundberg, J., Lysaker, O.M., 2015. An optimization framework for tracking droplets in fire water spray images. In: Proc. 56th Conf. Simul. Model. (SIMS 56), pp. 331–337. https://doi.org/10.3384/ecp15119331. October, 7-9, 2015, Linköping Univ. Sweden 119.

Mathworks, 2019. MathWorks. MATLAB 2019b. www.mathworks.com/products/matlab.

Myers, T., Trouvé, A., Marshall, A., 2018. Predicting sprinkler spray dispersion in FireFOAM. Fire Saf. J. 100, 93–102. https://doi.org/10.1016/j.firesaf.2018.07.008.

Myers, T.M., Marshall, A.W., 2016. A description of the initial fire sprinkler spray. Fire Saf. J. 84, 1–7. https://doi.org/10.1016/j.firesaf.2016.05.004.

NORSOK S-001, 2018. Technical Safety Rev. 5. Standards Norvegian Technology, Oslo.

Otsu, N., 1979. A threshold selection method from gray-level histograms. IEEE Trans. Syst. Man. Cybern. SMC- 9, 62–66.

Ren, N., Baum, H.R., Marshall, A.W., 2011. A comprehensive methodology for characterizing sprinkler sprays. Proc. Combust. Inst. 33, 2547–2554. https://doi.org/10.1016/j.proci.2010.06.107.

Roberts, T.A., 2004. Directed deluge system designs and determination of the effectiveness of the currently recommended minimum deluge rate for the protection of LPG tanks. J. Loss Prev. Process. Ind. 17, 103–109. https://doi.org/10.1016/j.jlp.2003.10.005.

Sheppard, D.T., 2002. Spray Characteristics of Fire Sprinklers. Nortwestern University.

Wighus, R., 2012. Droplet size, velocity and area distribution - deluge nozzles. Trondheim.

Zhou, X., D'Aniello, S.P., Yu, H.-Z., 2012. Spray characterization measurements of a pendent fire sprinkler. Fire Saf. J. 54, 36–48. https://doi.org/10.1016/j.firesaf.2012.07.007.

Zhou, X., 2015. Characterization of interactions between hot air plumes and water sprays for sprinkler protection. Proc. Combust. Inst. 35, 2723–2729. https://doi.org/10.1016/j.proci.2014.05.078.

Zlatanovic, L., Vreeburg, J., van der Hoek, J.P., Poznakovs, I., 2014. An experimental study on the spray characteristics of residential sprinklers under low-flow and low-pressure conditions. Fire Saf. J. 68, 30–40. https://doi.org/10.1016/j.firesaf.2014.05.018.